
DRAFT

CMS Physics Analysis Summary

The content of this note is intended for CMS internal use and distribution only

2012/06/20

Head Id: 131213

Archive Id: 130872:131214

Archive Date: 2012/06/20

Archive Tag: trunk

Measurement of the top polarization in the dilepton final state

The CMS Collaboration

Abstract

A measurement of the top quark polarization in $t\bar{t} \rightarrow \ell^+\ell^-$ events is performed in a data sample corresponding to a total integrated luminosity of 5.0 fb^{-1} collected by the CMS experiment in pp collisions at a centre-of-mass energy of 7 TeV at the LHC. The measured value in the helicity basis is $P_n = -0.035 \pm 0.028 \pm 0.056$, in agreement with the standard model expectation.

This box is only visible in draft mode. Please make sure the values below make sense.

PDFAuthor: Kevin Burkett, Oliver Gutsche, Sergo Jindariani, Vyacheslav Krutelyov, Jacob Linacre, Yanjun Tu
PDFTitle: Measurement of the top polarization in the dilepton final state
PDFSubject: CMS
PDFKeywords: CMS, physics, dilepton, top, polarization, polarisation, asymmetry

Please also verify that the abstract does not use any user defined symbols

1 Introduction

In the standard model (SM), tops and anti-tops in $t\bar{t}$ pair production are produced unpolarized from QCD. A small net polarization is expected in the SM from electroweak corrections to $t\bar{t}$ production. In physics beyond SM, couplings of the top to new particles can alter its polarization. Thus net polarization of the tops produced in $t\bar{t}$ production would be a good way to separate the new physics from the SM. In paper [1], the top polarization has been identified as an observable capable of distinguishing between different models which could be responsible for the large deviation of the $t\bar{t}$ forward-backward asymmetry observed in the Tevatron [2, 3].

The polarization of the top is reflected in the kinematic distributions of its daughters, because the top decays before hadronization effects can wash away this information. Among all the particles coming from the decay of the top, the charged lepton is most sensitive to the top's polarization. The top polarization P_n along a chosen axis \hat{n} can thus be measured from the angular distribution of the charged leptons from the decays, measured in the top quark rest frame:

$$\frac{1}{\Gamma} \frac{d\Gamma}{d \cos \theta_{l,n}} = \frac{1}{2} (1 + 2\kappa_l P_n \cos \theta_{l,n}), \quad (1)$$

where $\theta_{l,n}$ is the direction of the lepton with respect to \hat{n} and κ_l is the spin analyzing power of the lepton, equal to 1.0. In this analysis the helicity axis is used, where \hat{n} is given by the direction of the top in the $t\bar{t}$ CM frame.

This note presents a measurement of the top polarization in the helicity basis, using a data sample corresponding to an integrated luminosity of 5.0 fb^{-1} collected at $\sqrt{s} = 7 \text{ TeV}$ by the Compact Muon Solenoid (CMS) experiment at the LHC. A detailed description of the CMS detector can be found elsewhere [4]. Dilepton decays of the $t\bar{t}$ pair are used, and the top polarization is measured using the reconstructed objects. Because the reconstructed polarization is shaped by the reconstruction efficiency and resolution, we apply an unfolding technique to recover the parton-level distribution which can be compared with theoretical predictions.

2 Event samples, reconstruction, and selection

The data used for this measurement were collected using one of the ee , $e\mu$, or $\mu\mu$ high- p_T double-lepton triggers. Muon candidates are reconstructed using two algorithms that require consistent signals in the tracker and muon systems: one matches the extrapolated trajectories from the silicon tracker to signals in the muon system (tracker-based muons), and the second performs a global fit requiring consistent patterns in the tracker and the muon system (globally fitted muons) [5]. Electron candidates are reconstructed starting from a cluster of energy deposits in the electromagnetic calorimeter. The cluster is then matched to signals in the silicon tracker. A selection using electron identification variables based on shower shape and track-cluster matching is applied to the reconstructed candidates [6]. Electron candidates within $\Delta R \equiv \sqrt{(\Delta\eta)^2 + (\Delta\phi)^2} < 0.1$ from a muon are rejected to remove candidates due to muon bremsstrahlung and final-state radiation. Both electrons and muons are required to be isolated from other activity in the event. This is achieved by imposing a maximum allowed value of 0.15 on the ratio of the scalar sum of track transverse momenta and calorimeter transverse energy deposits within a cone of $\Delta R < 0.3$ around the lepton candidate direction at the origin (the transverse momentum of the candidate is excluded), to the transverse momentum of the candidate.

Event selection is applied to reject events other than those from $t\bar{t}$ in the dilepton final state. Events are required to have two opposite-sign, isolated leptons (e^+e^- , $e^\pm\mu^\mp$, or $\mu^+\mu^-$). Both leptons must have transverse momentum $p_T > 20 \text{ GeV}/c$, and the electrons (muons) must have $|\eta| < 2.5$ (2.4). The reconstructed lepton trajectories must be consistent with a common interaction vertex. In the rare case ($< 0.1\%$) of events with more than two such leptons, the two leptons with the highest p_T are selected. Events with an e^+e^- or $\mu^+\mu^-$ pair with invariant mass between 76 and 106 GeV/c^2 or below 12 GeV/c^2 are removed to suppress Drell–Yan (DY) events ($Z/\gamma^* \rightarrow \ell^+\ell^-$) as well as low mass dilepton resonances. The jets and the missing transverse energy E_T^{miss} are reconstructed with a particle-flow technique [7]. The anti- k_T clustering algorithm [8] with a distance parameter of 0.5 is used for jet clustering. At least two jets with $p_T > 30 \text{ GeV}/c$ and $|\eta| < 2.5$, separated by $\Delta R > 0.4$ from leptons passing the analysis selection, are required in each event. At least one of these jets is required to be consistent with coming from the decay of heavy flavor hadrons and be identified as a b jet by the Combined Secondary Vertex Medium Point (CSVM) b-tagging algorithm [9], which is based on the reconstruction of a secondary vertex. The E_T^{miss} in the event is required to exceed 30 GeV , consistent with the presence of two undetected neutrinos.

Signal and background events are generated using the MADGRAPH 4.4.12 [10] and PYTHIA 6.4.22 [11] event generators. For $t\bar{t}$ events, POWHEG with PYTHIA is used for the $t\bar{t} \rightarrow \ell^+\ell^-$ component (corresponding to dileptonic $t\bar{t}$, including τ leptons only when they also decay leptonically), while all other $t\bar{t}$ decay modes, denoted $t\bar{t} \rightarrow \text{other}$ is generated using MADGRAPH. The samples of DY with $M_{\ell\ell} > 50 \text{ GeV}/c^2$, diboson (WW, WZ, and ZZ only: the contribution from $W\gamma$ is assumed to be negligible), and single top quark events are generated using MADGRAPH. The DY event samples with $M_{\ell\ell} < 50 \text{ GeV}/c^2$ are generated using PYTHIA.

Events are then simulated using a GEANT4-based model [12] of the CMS detector, and finally reconstructed and analyzed with the same software used to process collision data. The cross section for $t\bar{t}$ production is taken from a recent CMS measurement [13], while next-to-leading order (NLO) cross sections are used for the remaining SM background samples.

With the steadily increasing LHC instantaneous luminosity, the mean number of interactions in a single bunch crossing also increased over the course of data taking, reaching about 15 at the end of the 2011 running period. In the following, the yields of simulated events are weighted such that the distribution of reconstructed vertices observed in data is reproduced. The efficiency for events containing two leptons satisfying the analysis selection to pass at least one of the double-lepton triggers is measured with a tag-and-probe method to be approximately 100%, 95%, and 90% for the ee , $e\mu$, and $\mu\mu$ triggers, respectively [14], and corresponding weights are applied to the simulated event yields. In addition, b-tagging scale factors are applied to simulated events for each jet, to account for the difference between b-tagging efficiencies in data and simulation [9].

3 Event yields and top polarization at reconstruction level

The observed and simulated yields after the event selection are listed in Table 1. The yields are dominated (92%) by top-pair production in the dilepton final state, with the largest background coming from single top production. The $t\bar{t} \rightarrow \ell^+\ell^-$ yields are normalized such that the total simulated yield matches the number of events in data. Comparisons between data and the simulation for the number of b tagged jets and the reconstructed top quark mass (M_t) are shown in Figure 1.

Table 1: The observed and simulated yields after the event selection described in the text. Uncertainties are statistical only. The systematic uncertainties on the simulated yields are given in Section 6. Where the simulated yields are zero, upper limits are given based on the weighted yield, had one of the simulated events passed the selection.

Sample	ee	$\mu\mu$	$e\mu$	all
$t\bar{t} \rightarrow \ell^+\ell^-$	1791.7 ± 4.4	2127.3 ± 4.7	5069.4 ± 7.3	8988.5 ± 9.7
$t\bar{t} \rightarrow \text{other}$	32.5 ± 2.9	4.8 ± 1.1	53.3 ± 3.6	90.7 ± 4.8
W + jets	< 1.9	4.7 ± 3.3	4.7 ± 3.4	9.4 ± 4.7
DY \rightarrow ee	52.3 ± 5.8	< 0.6	< 0.6	52.3 ± 5.8
DY \rightarrow $\mu\mu$	< 0.6	72.8 ± 6.5	1.6 ± 0.9	74.4 ± 6.5
DY \rightarrow $\tau\tau$	17.6 ± 3.3	8.7 ± 2.2	18.7 ± 3.2	45.0 ± 5.1
Di-boson	10.6 ± 0.5	13.0 ± 0.5	24.0 ± 0.7	47.6 ± 1.0
Single top	84.9 ± 2.3	101.2 ± 2.4	252.1 ± 3.9	438.2 ± 5.1
Total (simulation)	1989.6 ± 8.8	2332.6 ± 9.3	5423.8 ± 10.3	9746.0 ± 16.4
Data	1961	2373	5412	9746

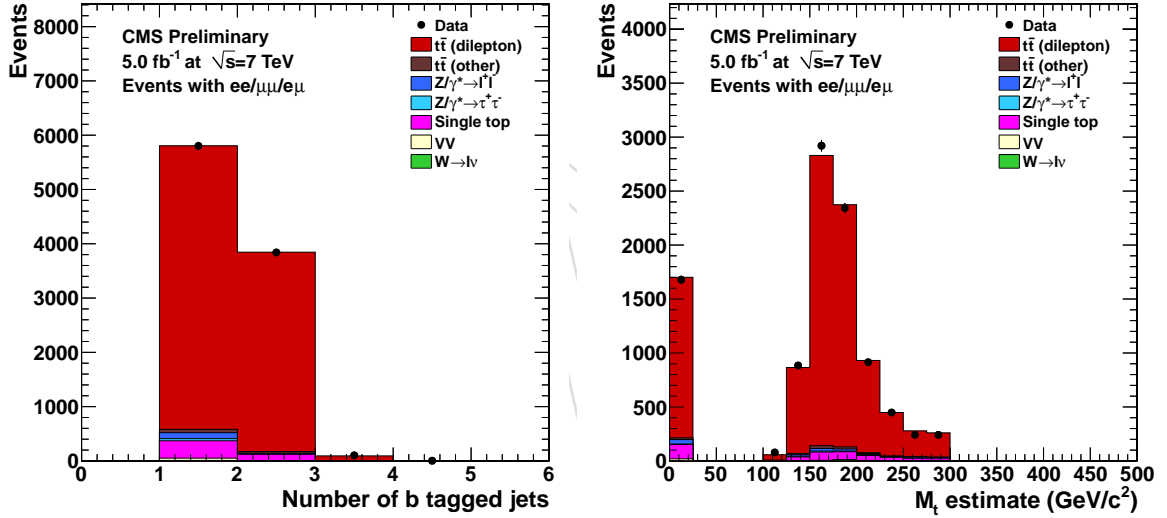


Figure 1: Comparison of data and simulation for number of b tagged jets (left) and reconstructed top quark mass (right), where events with no solution found are filled in the first bin.

From Equation 1, the top polarization can be extracted from

$$P_n = \frac{N(\cos(\theta_l^+) > 0) - N(\cos(\theta_l^+) < 0)}{N(\cos(\theta_l^+) > 0) + N(\cos(\theta_l^+) < 0)},$$

86 where θ_l^+ is the production angle of the positively charged lepton in the rest frame of its parent
 87 top, with respect to the direction of the parent top in the $t\bar{t}$ rest frame. Equivalently, P_n can be
 88 measured using θ_l^- , but in this analysis θ_l^+ is always used.

89 Measurement of this observable requires reconstruction of the $t\bar{t}$ system. Each event has two
 90 neutrinos, and there is also ambiguity in combining b jets with leptons. The analytical matrix
 91 weighting technique [15] is used to find a probable solution. Each event is reconstructed using
 92 a range of possible M_t values from 100-300 GeV/c^2 in 1 GeV/c^2 steps. The M_t hypothesis with

93 the maximum averaged weight over possible solutions is taken, and the $t\bar{t}$ kinematics are then
 94 taken from the solution with largest weight. Approximately 17% of events have no solution
 95 found, and are thus not used in the measurement of the top polarization.

96 A comparison of the $\cos(\theta_l^+)$ distributions in data and simulation is shown in Figure 2. The
 97 resulting value of P_n at reconstruction level is 0.083 ± 0.011 in data and 0.103 ± 0.002 in the
 98 simulation, where the uncertainties are statistical only. The remainder of this note focuses on
 99 making the necessary corrections to obtain P_n at parton-level, due to the presence of back-
 100 ground events and resolution and acceptance effects.

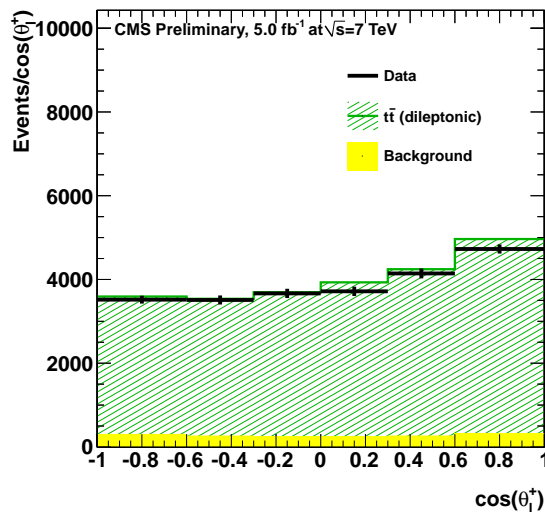


Figure 2: The reconstruction level $\cos(\theta_l^+)$ distribution, for data and the simulation. The simulated events are divided into $t\bar{t} \rightarrow \ell^+\ell^-$ and background, where the background consists of the categories other than $t\bar{t} \rightarrow \ell^+\ell^-$ in Table 1.

101 4 Background estimation

102 The simulation is used to predict the background event yields and shapes. We use methods
 103 based on data to cross-check these estimates for the background contributions from events with
 104 misidentified leptons and from $DY \rightarrow ee/\mu\mu$ events. However, the dependence of the measured
 105 top polarization on the background normalization is small, and in Section 6 the systematic
 106 uncertainty is estimated based on changing the normalization of each component by up to
 107 100%.

108 A misidentified lepton is defined as a lepton candidate not originating from a prompt decay,
 109 such as a lepton from semileptonic b or c quark decays, a muon from a pion or kaon decay, an
 110 unidentified photon conversion, or a pion misidentified as an electron. The background from
 111 events with misidentified leptons is predicted based on the number of events in data with a
 112 candidate lepton that can pass only loosened selection criteria [16]. Using a measurement of
 113 the fraction of such “loose” leptons that go on to pass the selection requirements, the number of
 114 misidentified leptons in the event sample can be estimated. The resulting prediction is 138^{+281}_{-138}
 115 events, including both statistical and systematic uncertainties. The simulated yield is $100.1 \pm$
 116 6.7 , in reasonable agreement.

117 The estimation method for $DY \rightarrow ee/\mu\mu$ events [17] is based on counting the number of Z

118 candidates in the Z veto region (after subtracting the number of non Z events estimated using
 119 the number of $e\mu$ events), and multiplying this number by the ratio of simulated DY yields
 120 outside to inside the Z veto region. The result is an estimate of 142.4 ± 15.0 $DY \rightarrow ee/\mu\mu$ events.
 121 The result is thus consistent with the simulated prediction of 126.7 ± 8.7 from Table 1.

122 5 Unfolding

123 The measured distribution is distorted from the true underlying distribution by the limited ac-
 124 ceptance of our detector and the finite resolution of the measurement. In order to correct data
 125 for these effects, we apply the unfolding procedure which yields the ‘‘parton-level’’ $\cos(\theta_l^+)$
 126 distribution. This distribution represents the differential cross-section in $\cos(\theta_l^+)$, and is nor-
 127 malized to unity.

128 Choice of a binning scheme for the distribution is motivated by the desire to minimize bin-
 129 to-bin oscillations caused by statistical fluctuations. The bin size is variable and is chosen to
 130 ensure similar level of statistics in each bin of the distribution. A summary of the binning is
 131 provided in Table 2.

Table 2: Binning used in the distributions of $\cos(\theta_l^+)$.

B1	B2	B3	B4	B5	B6
[-1.0,-0.6]	[-0.6,-0.3]	[-0.3,-0.0]	[0.0, 0.3]	[0.3, 0.6]	[0.6, 1.0]

132 The background-subtracted measured distribution \vec{b} is related to the underlying parton-level
 133 distribution \vec{x} by the matrix equation $\vec{b} = SA\vec{x}$, where A is a diagonal matrix describing the
 134 acceptance in each bin of the measured distribution, and S is a non-diagonal smearing matrix
 135 describing the migration of events between bins due to the detector resolution and reconstruc-
 136 tion techniques. The A and S matrices are modeled using the NLO POWHEG-PYTHIA $t\bar{t}$ sample,
 137 and are shown in Fig. 3. The smearing effects are quite large due to the uncertainties of top
 138 reconstruction. However, most of the large values lie close to the diagonal, meaning there is
 139 little migration between far-apart bins.

140 We employ a regularized ‘‘unfolding’’ algorithm based on singular value decomposition (SVD) [18],
 141 which is implemented in the RooUnfold package. Effects of large statistical fluctuations in the
 142 algorithm are greatly reduced by introducing a regularization term to the unfolding proce-
 143 dure. The full covariance matrix is used in the evaluation of the statistical uncertainty of the
 144 measured asymmetry.

145 We verify that the unfolding procedure is able to correctly unfold distributions with different
 146 levels of asymmetry. In order to do this, we re-weight generated $t\bar{t}$ events according to a linear
 147 function of $\cos(\theta_l^+)$: $\text{weight}=1+K \cos(\theta_l^+)$. The parameter K is varied between -0.5 and 0.5 in
 148 steps of 0.2, introducing a polarization of up to 40%, far more than is expected in $t\bar{t}$ events. For
 149 each value of K , we generate 2000 pseudo-experiments, in which the number of events in each
 150 bin of the distribution is fluctuated according to Poisson statistics, and then the distribution
 151 is unfolded. The average value of the asymmetry in 2000 pseudo-experiments is compared
 152 to the original true-level value. We find a linear behavior of this distribution, suggesting that
 153 non-SM asymmetry values will also be measured correctly. The offsets and slopes obtained in
 154 the linear function fit are -0.004 ± 0.009 and 1.031 ± 0.053 , respectively. We also look at the
 155 distribution of the pulls in the set of pseudo-experiments and fit it to gaussian function. We
 156 find a small bias leading to asymmetry changes of up to 1%, and assign it as an additional
 157 systematic uncertainty associated with unfolding bias.

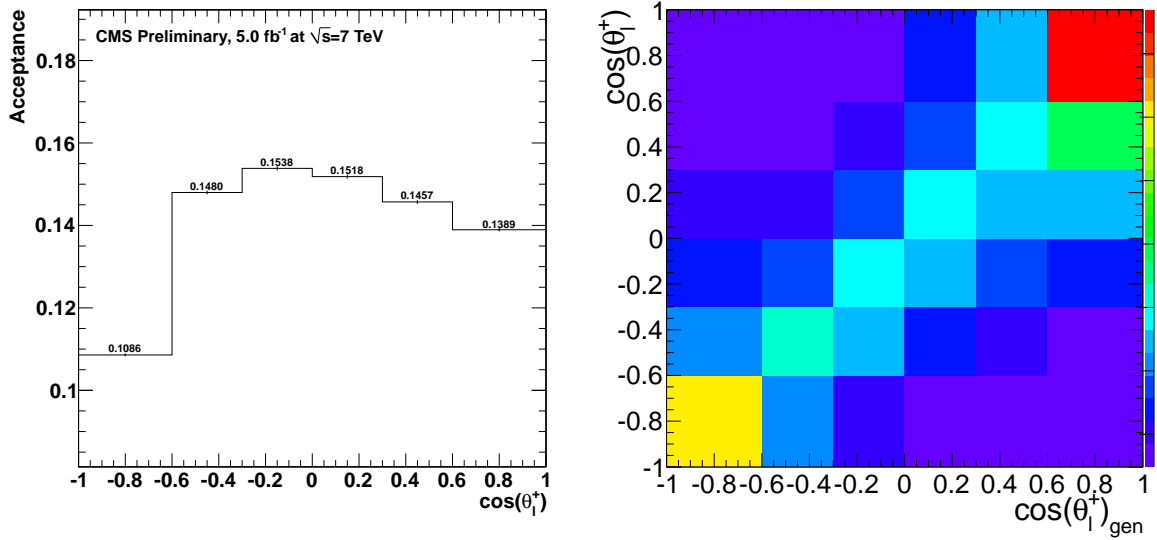


Figure 3: Acceptance matrix bins (left) and smearing effects due to the uncertainties of top reconstruction (right).

6 Systematic uncertainties

158

159 The systematic uncertainty associated with the jet and E_T^{miss} energy scale can directly affect
 160 the shape of the asymmetry distributions. We evaluate this uncertainty, assuming a 7.5% un-
 161 certainty to the hadronic energy scale after jet corrections have been applied [19]. A similar
 162 uncertainty on the lepton energy scale is evaluated by shifting the electron energies by $\pm 0.3\%$
 163 (the uncertainty on muon energies is negligible in comparison). We also evaluate a systematic
 164 uncertainty on the choice of M_t scan range in the solver.

165 There are also a number of systematic uncertainties due to the background subtraction and
 166 unfolding used to produce the parton level measurement. Given the uncertainties of the data
 167 driven background estimates described in Section 4, the uncertainty associated with the back-
 168 ground estimate is obtained by changing the background yields. We vary the backgrounds
 169 from DY and misidentified leptons by 100%. In addition, we vary the single top background
 170 by 50%. The systematic uncertainty from the $t\bar{t}$ modeling is estimated by applying unfolding
 171 derived using MC@NLO $t\bar{t}$ to POWHEG-PYTHIA events, and taking the difference in the result
 172 compared to that for the POWHEG-PYTHIA derived unfolding. We also assess the systematics
 173 due to the shower matching, factorization and renormalization scales, the top mass used in sim-
 174 ulation, the b -tagging efficiency, the trigger efficiency, the lepton ID efficiency and the pile-up
 175 reweighting. The systematic uncertainties on the unfolded P_n measurement are summarized
 176 in Table 3, combining in quadrature to a total systematic uncertainty of 0.056.

Table 3: Systematic uncertainties.

JES	lepton energy scale	M_t scan range	background	modeling	matching
0.043	0.001	0.024	0.009	0.014	0.004
scale	simulated M_t	b -tagging eff.	Trig eff. and lep ID	pile-up	Total
0.007	0.019	0.001	0.000	0.002	0.056

7 Results and summary

The background-subtracted and unfolded $\cos(\theta_1^+)$ distribution for $t\bar{t} \rightarrow \ell^+\ell^-$ events is shown in Figure 4. The measured value of P_n at parton-level is $-0.035 \pm 0.028 \pm 0.056$, while the $t\bar{t}$ parton level prediction obtained from POWHEG-PYTHIA simulation is 0.003 ± 0.0004 . The correlation between bins as a result of the unfolding procedure is accounted for in the evaluation of the uncertainties.

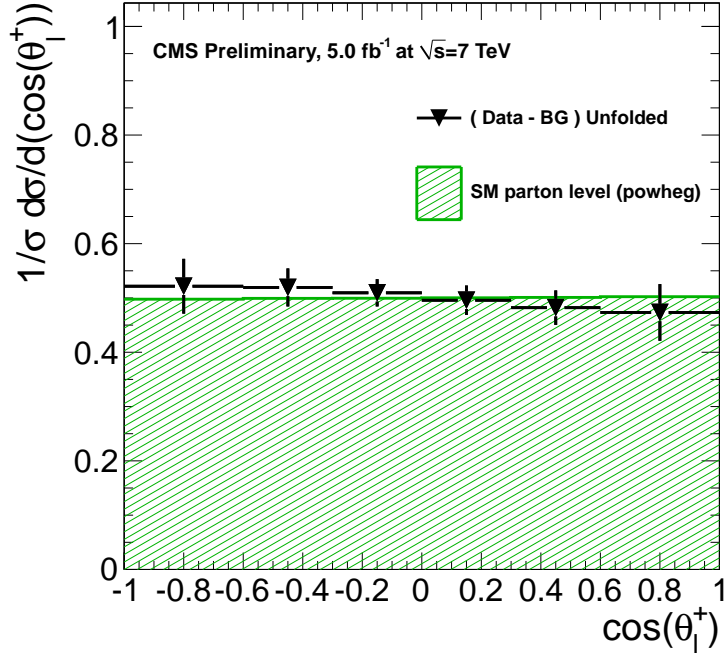


Figure 4: Background-subtracted and unfolded $\cos(\theta_1^+)$ distribution. The error bars include both statistical and systematic uncertainties. Note that the bin values are correlated due to the unfolding.

The measured value of P_n is consistent with the POWHEG-PYTHIA value, and we thus observe no significant deviation from the SM expectation.

8 Acknowledgements

We would like to thank Dr. T. Liu for fruitful discussions and helpful correspondence on the theory part. We are also very grateful to Dr. T. Schwarz and Dr. D. Mietlicki for fruitful discussions. We congratulate our colleagues in the CERN accelerator departments for the excellent performance of the LHC machine. We thank the technical and administrative staff at CERN and other CMS institutes, and acknowledge support from: FMSR (Austria); FNRS and FWO (Belgium); CNPq, CAPES, FAPERJ, and FAPESP (Brazil); MES (Bulgaria); CERN; CAS, MoST, and NSFC (China); COLCIENCIAS (Colombia); MSES (Croatia); RPF (Cyprus); MoER, SF0690030s09 and ERDF (Estonia); Academy of Finland, MEC, and HIP (Finland); CEA and CNRS/IN2P3 (France); BMBF, DFG, and HGF (Germany); GSRT (Greece); OTKA and NKTH (Hungary); DAE and DST (India); IPM (Iran); SFI (Ireland); INFN (Italy); NRF and WCU (Korea); LAS (Lithuania); CINVESTAV, CONACYT, SEP, and UASLP-FAI (Mexico); MSI (New Zealand); PAEC (Pakistan); MSHE and NSC (Poland); FCT (Portugal); JINR (Armenia, Belarus, Georgia, Ukraine, Uzbekistan); MON, RosAtom, RAS and RFBR (Russia); MSTD (Ser-

199 bia); SEIDI and CPAN (Spain); Swiss Funding Agencies (Switzerland); NSC (Taipei); TUBITAK
200 and TAEK (Turkey); STFC (United Kingdom); DOE and NSF (USA).

201 References

- 202 [1] D. Krohn, T. Liu, J. Shelton et al., “A Polarized View of the Top Asymmetry”, *Phys.Rev.*
203 **D84** (2011) 074034, doi:10.1103/PhysRevD.84.074034, arXiv:1105.3743.
- 204 [2] CDF Collaboration, “Forward-Backward Asymmetry in Top Quark Production in $p\bar{p}$
205 Collisions at $\sqrt{s} = 1.96$ TeV”, *Phys.Rev.Lett.* **101** (2008) 202001, arXiv:0806.2472.
- 206 [3] D0 Collaboration, “First measurement of the forward-backward charge asymmetry in top
207 quark pair production”, *Phys.Rev.Lett.* **100** (2008) 142002, arXiv:0712.0851.
- 208 [4] CMS Collaboration, “The CMS experiment at the CERN LHC”, *JINST* **3** (2008) S08004,
209 doi:10.1088/1748-0221/3/08/S08004.
- 210 [5] CMS Collaboration, “Performance of muon identification in pp collisions at $\sqrt{s} = 7$ TeV”,
211 CMS Physics Analysis Summary CMS-PAS-MUO-10-002, (2010).
- 212 [6] CMS Collaboration, “Electron Reconstruction and Identification at $\sqrt{s} = 7$ TeV”, CMS
213 Physics Analysis Summary CMS-PAS-EGM-10-004, (2010).
- 214 [7] CMS Collaboration, “Commissioning of the Particle-Flow Reconstruction in
215 Minimum-Bias and Jet Events from pp Collisions at 7 TeV”, CMS Physics Analysis
216 Summary CMS-PAS-PFT-10-002, (2010).
- 217 [8] M. Cacciari, G. Salam, and G. Soyez, “The anti- k_T jet clustering algorithm”, *JHEP* **04**
218 (2008) 063, doi:10.1088/1126-6708/2008/04/063, arXiv:0802.1189.
- 219 [9] CMS Collaboration, “Measurement of the b-tagging efficiency using $t\bar{t}$ events”, CMS
220 Physics Analysis Summary CMS-PAS-BTV-11-003, (2011).
- 221 [10] J. Alwall, P. Demin, S. de Visscher et al., “MadGraph/MadEvent v4: the new web
222 generation”, *JHEP* **09** (2007) 028, doi:10.1088/1126-6708/2007/09/028,
223 arXiv:0706.2334.
- 224 [11] T. Sjöstrand, S. Mrenna, and P. Skands, “PYTHIA 6.4 physics and manual”, *JHEP* **05**
225 (2006) 026, doi:10.1088/1126-6708/2006/05/026, arXiv:0706.2334.
- 226 [12] S. Agostinelli et al., “GEANT4 – a simulation toolkit”, *Nucl. Instr. and Meth. A* **506** (2003)
227 250, doi:10.1016/S0168-9002(03)01368-8.
- 228 [13] CMS Collaboration, “Measurement of the $t\bar{t}$ production cross section in pp collisions at
229 7 TeV in lepton + jets events using b -quark jet identification”, *Phys. Rev. D* **84** (2011)
230 092004, doi:10.1103/PhysRevD.84.092004, arXiv:1108.3773.
- 231 [14] CMS Collaboration, “Search for heavy, top-like quark pair production in the dilepton
232 final state in pp collisions at $\sqrt{s} = 7$ TeV”, *Submitted to PLB* (2012) arXiv:1203.5410.
- 233 [15] CMS Collaboration Collaboration, “Measurement of the $t\bar{t}$ production cross section
234 and the top quark mass in the dilepton channel in pp collisions at $\sqrt{s} = 7$ TeV”, *JHEP*
235 **1107** (2011) 049, arXiv:1105.5661.

- 236 [16] CMS Collaboration, “Search for new physics with same-sign isolated dilepton events
237 with jets and missing transverse energy at the LHC”, *JHEP* **6** (2011) 077,
238 doi:10.1007/JHEP06(2011)077, arXiv:1104.3168.
- 239 [17] CMS Collaboration Collaboration, “First Measurement of the Cross Section for
240 Top-Quark Pair Production in Proton-Proton Collisions at $\sqrt{s}=7$ TeV”, *Phys.Lett.*
241 **B695** (2011) 424–443, arXiv:1010.5994.
- 242 [18] A. Hocker and V. Kartvelishvili, “SVD approach to data unfolding”, *Nucl.Instrum.Meth.*
243 **A372** (1996) 469–481, doi:10.1016/0168-9002(95)01478-0,
244 arXiv:hep-ph/9509307.
- 245 [19] CMS Collaboration, “Determination of the Jet Energy Scale in CMS with pp Collisions at
246 $\sqrt{s} = 7$ TeV”, CMS Physics Analysis Summary CMS-PAS-JME-10-010, (2010).

DRAFT